Insights on the site-selective fragmentation of CF_2Cl_2 and CH_2Cl_2 at the chlorine K-edge from ab initio calculations

Tenorio, Bruno Nunes Cabral; Oliveira, Ricardo R.; Coriani, Sonia

Published in:
Chemical Physics

Link to article, DOI:
10.1016/j.chemphys.2021.111226

Publication date:
2021

Document Version
Peer reviewed version

Journal Pre-proofs

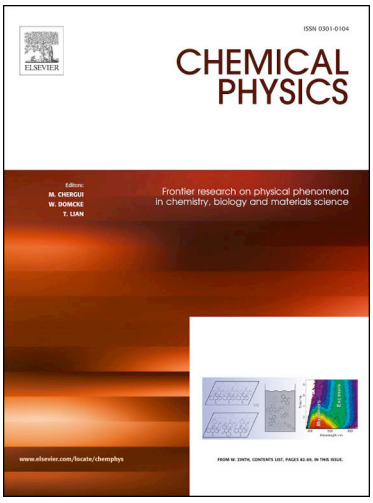

Insights on the site-selective fragmentation of CF_2Cl_2 and CH_2Cl_2 at the chlorine K-edge from *ab initio* calculations

Bruno Nunes Cabral Tenorio, Ricardo R. Oliveira, Sonia Coriani

PII: S0301-0104(21)00137-3
DOI: https://doi.org/10.1016/j.chemphys.2021.111226
Reference: CHEMPH 111226

To appear in: *Chemical Physics*

Received Date: 12 December 2020
Accepted Date: 24 April 2021

Please cite this article as: B.N. Cabral Tenorio, R.R. Oliveira, S. Coriani, Insights on the site-selective fragmentation of CF_2Cl_2 and CH_2Cl_2 at the chlorine K-edge from *ab initio* calculations, *Chemical Physics* (2021), doi: https://doi.org/10.1016/j.chemphys.2021.111226

Insights on the site-selective fragmentation of CF_2Cl_2 and CH_2Cl_2 at the chlorine K-edge from *ab initio* calculations

Bruno Nunes Cabral Tenorio,*,† Ricardo R. Oliveira,‡ and Sonia Coriani†

†*DTU Chemistry - Department of Chemistry, Technical University of Denmark, Kemitorvet Bldg 207, 2800 Kongens Lyngby, Denmark*

‡*UFRJ - Universidade Federal do Rio de Janeiro, Instituto de Química, Av. Athos da Silveira Ramos, 149, Rio de Janeiro - RJ, 21941-909, Brasil*

E-mail: brncat@dtu.dk

Abstract

A theoretical study of CF_2Cl_2 and CH_2Cl_2 photoabsorption spectra and photofragmentation profiles at the chlorine K-edge is presented. We simulated the NEXAFS spectra at the Core-Valence Separated Coupled Cluster Singles and Doubles (CVS-CCSD) level and interpreted the photofragmentation profile in terms of the potential energy surfaces (PES) computed at the complete active space self-consistent field (CASSCF) level along the C–Cl bond cleavage for the $1s_{Cl} \rightarrow \sigma^*_{C-Cl}$, $1s_{Cl} \rightarrow 7b_2$, and $1s_{Cl} \rightarrow \infty$ states. The PES of CF_2Cl_2 shows that the chlorine's $1s \rightarrow \sigma^*$ transition tends to fragment into the CF_2Cl^* radical and the Cl ($1s^1 2s^2 2p^6 3s^2 3p^6$) excited atom, whereas the $1s_{Cl} \rightarrow 7b_2$ and $1s_{Cl} \rightarrow \infty$ states are less prone to undergo this fragmentation channel. The same tendency was observed for the CH_2Cl_2 molecule, suggesting that the F atom has little influence on the PES.

Introduction

The development of new synchrotron facilities and free-electron-laser light sources has enabled a deeper understanding the interaction of X-ray radiation with polyatomic molecules and solids and, consequently, the damage caused to the target systems.[1–4] Besides, there is technological interest in hard X-ray sources because they can be applied in the characterization of materials and heterogeneous media.[5–7] Also, photoexcitation of a molecule from a deep core shell is normally very unstable and the corresponding excited states have a short lifetime, from tenths to dozens of femtoseconds.[1,2,8–12] The main path of relaxation of the core hole in molecules is by emission of Auger electrons. When an electron from a core orbital is ejected, a highly localized inner-shell state is formed. As a consequence, the fragmentation process after Auger relaxation can be site-selective, resulting in the cleavage of a specific chemical bond.[1,2,13,14]

The decay mechanism is well established for atoms. In molecules, however, there are several possibilities, especially for large systems such as organic molecules and radicals.[1,3] Recently, several efforts have been made to describe and understand the molecular rearrangement, fragmentation mechanism and/or excited-state dynamics induced by X-ray absorption.[1,2,8,10,13,15–19] For example, the ultrafast ring-opening reaction of 1,3-cyclohexadiene was investigated using femtosecond soft X-ray spectroscopy near the carbon K-edge, combined with Time-Dependent Density Functional Theory (TDDFT) calculations.[9] Another interesting example is the $\pi\pi^*$-$n\pi^*$ internal conversion in the nucleobase thymine monitored by absorption at the O1s–n resonance.[17] Furthermore, site-selective fragmentation induced by K-shell core excitation has been recently observed in N-methylacetamide[20] and 2-Br-pyrimidine.[21] Even for complex molecules such as methionine enkephalin peptide, near-edge X-ray absorption combined with mass spectrometry revealed that the excitation at S2p $\rightarrow \sigma^*$ resonance leads to a site-selective dissociation, whereas above core ionization the fragmentation is no longer selective.[3]

In general, vacuum ultra violet (VUV) spectroscopy is not able to produce site-specific

data on photochemistry dynamics as X-ray techniques do, especially when monitoring bond dissociation in excited states potential energy surfaces.[2,3,13,22] Despite having emerged decades ago, site-specific fragmentation induced by soft X-ray is still very relevant nowadays.[23–25] Several works from different research groups have recently been published that explore this fragmentation as "chemical scissors" for organic and small relevant biochemical systems.[3,26–28] In particular, in the case of small halogenated organic compounds, distinct ultrafast fragmentation channels at different edges have been reported during the last few years.[2,8,10,11,13,15,16,22,29–34] The Cl $2p_{3/2} \rightarrow \sigma^*$ resonance in CH_2Cl_2 induces ultrafast C–Cl bond cleavage, with atomic and molecular decay as competitive channels,[13,29] whereas selectivity was not obtained for the CCl_4 molecule.[29,31] For the CF_3Cl molecule, the C1s $\rightarrow$ σ^* resonance leads to the C–Cl bond-breaking, whereas the resonance at Cl 2p exhibits a complex fragmentation mechanism.[35] Carbon atoms in distinct chemical environments can also lead to selective fragmentation. In the CH_2FCF_3 molecule, C1s(H_2F) excitation induces the C–F cleavage, whereas C1s(F_3) leads to a C-C bond cleavage.[10] The F1s $\rightarrow \sigma^*$ excitation in CH_3F also induces the C-F bond to break and the same was reported for C1s core excitation.[36] Even if ion coincidence and time-resolved spectroscopic techniques reveal some ultrafast fragmentation features, *ab initio* quantum chemistry calculations are often applied in order to obtain insights on this complex process.

In this work we investigated the excited states of CF_2Cl_2 and CH_2Cl_2 at Cl K-edge, in order to shed light on the first steps of their site-selective fragmentation induced by X-rays. Based on the CF_2Cl_2 PES computed at the CASSCF level, we describe how the Cl 1s$\rightarrow \sigma^*$ electronic transition goes toward fragmentation into the CF_2Cl^* radical and the excited $Cl^*(1s^12s^22p^63s^23p^6)$ atom, whereas the Cl 1s$\rightarrow 7b_2$ (core excited) and the Cl $1s \rightarrow \infty$ (core ionized) states have a weaker tendency to follow this fragmentation channel. Since autoionization takes place in the femtosecond time scale, the C-Cl cleavage must occur in the femtosecond domain in order to produce atomic Auger decay. Auger-cascade decay has been observed for Cl 1s excitation of gaseous CH_2Cl_2,[11] generating chlorine fragments with

charges up to +4, while those with charges only up to +2 were observed following Cl 2p excitation.[37] In accordance with the ultrafast C-Cl fragmentation picture, the unstable species $Cl(1s^1 2s^2 2p^6 3s^2 3p^6)$ decays via Auger-cascade process after the C-Cl bond is broken, generating multi-charged atomic chlorine ions. Besides the CASSCF computations, the (frozen-core) core-valence separated coupled cluster singles and double (CVS-CCSD) method[38–40] was used to simulate the NEXAFS spectra at the Chlorine K edge and to assign the spectral features in the experimental counterpart.

Computational Details

We performed a series of high-level *ab initio* quantum mechanical calculations using the frozen-core core-valence separated coupled cluster singles and doubles (fc-CVS-CCSD)[40] and the complete active space self-consistent field (CASSCF)[41] approaches. Specifically, we used fc-CVS-CCSD[38–40] to obtain accurate NEXAFS spectra of CF_2Cl_2 and CH_2Cl_2 at the K-edge of the Cl atom and at ground state equilibrium geometry. The ground state equilibrium geometries were taken from the NIST compilation.[42] The photofragmentation profiles around the Cl K-edge region of both chlorinated molecules were interpreted in terms of the potential energy surfaces computed at the CASSCF level. The CASSCF and CCSD calculations were performed with the Molpro[43] and with the Qchem program package,[44] respectively. The aug-cc-pCVDZ basis set[45] was used in all calculations.

Minimum energy pathways of the C–Cl bond dissociation for the chlorinated molecules were obtained; i.e., for a given C-Cl distance, all other coordinates (geometry and orbitals) were optimized. For a given geometrical arrangement, the electronic states were calculated following the inner-shell complete active space self-consistent field protocol,[22,30,46–48] where the inner-shell orbitals are relaxed keeping all other orbitals frozen in the first step of the calculation. Then, all the other coordinates, including the geometry and the active orbitals, are relaxed with the previously optimized inner shell orbitals kept frozen. The procedure is

iteratively repeated until the total energy of the corresponding inner-shell state converges. Basically, one freezes selected orbitals at different steps to avoid the variational collapse of the wave function to a low-lying electronic state of the molecule or ion.

Results and discussion

NEXAFS of the CF_2Cl_2 and CH_2Cl_2 molecules

In Fig. 1, we present simulated NEXAFS spectrum at fc-CVS-CCSD level of the CF_2Cl_2 and CH_2Cl_2, plotted alongside the experimental results.[11,32] For a better comparison, a Gaussian convolution with a full-width-at-half-maximum (FWHM) of 0.5 eV was applied. An *ad hoc* shift of +3 eV has been applied to the computed excitation energies to better compare the calculations with the experimental data. The main peaks of Fig. 1 are collected in Tables 1 and 2, where they are compared with experimental data.

Table 1: CF_2Cl_2: excitation energies (eV) and oscillator strengths of the Cl K-edge states computed at the fc-CVS-CCSD/aug-cc-pCVDZ level. In parentheses we show the computed excitation energies shifted by +3 eV to better compare with the experimental data.

Peak	State Symmetry	Assignment	Energy (eV)		Oscillator strength
			fc-CVS-CCSD (+3) eV	Experiment[32]	
A	A_1	Cl 1s $\rightarrow \sigma^*_{C-Cl}$	2819.5 (2822.5)	2823	3.53×10^{-3}
A	B_1	Cl 1s $\rightarrow \sigma^*_{C-Cl}$	2819.5 (2822.5)	2823	9.62×10^{-3}
B	A_1	Cl 1s $\rightarrow$ Rydberg p	2823.4 (2826.4)	-	1.36×10^{-4}
B	B_1	Cl 1s $\rightarrow$ Rydberg p	2823.4 (2826.4)	-	5.66×10^{-4}
C	B_2	Cl 1s $\rightarrow$ Rydberg p	2824.8 (2827.8)	2827	4.20×10^{-3}
C	A_1	Cl 1s $\rightarrow$ Rydberg p	2824.8 (2827.8)	2827	2.31×10^{-3}
C	B_1	Cl 1s $\rightarrow$ Rydberg p	2824.8 (2827.8)	2827	9.68×10^{-4}
IP		Cl 1s (A_1) $\rightarrow \infty$ / Cl 1s (B_1) $\rightarrow \infty$	2826.8 (2829.8)	-	-

Table 2: CH_2Cl_2: excitation energies (eV) and oscillator strengths of the Cl K-edge states computed at the fc-CVS-CCSD/aug-cc-pCVDZ level. In parentheses we show the computed excitation energies shifted by +3 eV to better compare with the experimental data.

Peak	State Symmetry	Assignment	Energy (eV) fc-CVS-CCSD (+3) eV	Energy (eV) Experiment [11]	Oscillator strength
A	A_1	Cl 1s $\rightarrow \sigma^*_{C-Cl}$	2819.5 (2822.5)	2822.9	3.73×10^{-3}
A	B_1	Cl 1s $\rightarrow \sigma^*_{C-Cl}$	2819.5 (2822.5)	2822.9	8.76×10^{-3}
B	A_1	Cl 1s $\rightarrow$ Rydberg d	2822.4 (2825.4)	-	3.56×10^{-4}
B	B_1	Cl 1s $\rightarrow$ Rydberg d	2822.4 (2825.4)	-	1.7×10^{-5}
C	A_1	Cl 1s (a_1) $\rightarrow$ Rydberg p	2823.5 (2826.5)	2826.5	2.21×10^{-3}
C	B_2	Cl 1s (a_1) $\rightarrow$ Rydberg p	2823.5 (2826.5)	2826.5	1.35×10^{-3}
C	A_1	Cl 1s (a_1) $\rightarrow$ Rydberg p	2823.7 (2826.7)	2826.5	7.37×10^{-4}
IP		Cl 1s (A_1) $\rightarrow \infty$ / Cl 1s (B_1) $\rightarrow \infty$	2826.0 (2829.0)	-	-

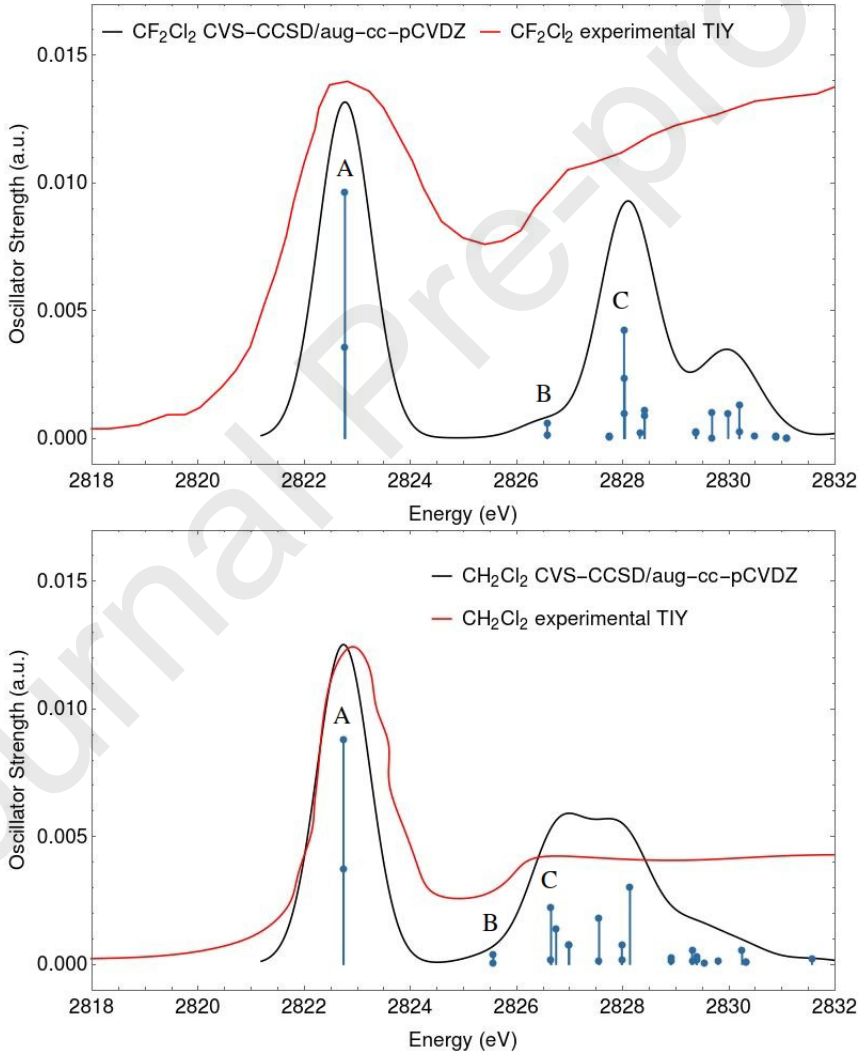

Figure 1: Black: NEXAFS spectrum of the CF_2Cl_2 (top) and CH_2Cl_2 (bottom) molecules at the Cl K-edge computed at the CVS-CCSD/aug-cc-pCVDZ level. The computed spectra were broadened with Gaussian functions with a FWHM of 0.5 eV. The TIY experimental spectrum by Gomes et al. [32] and Lago et al. [11] are plotted in red.

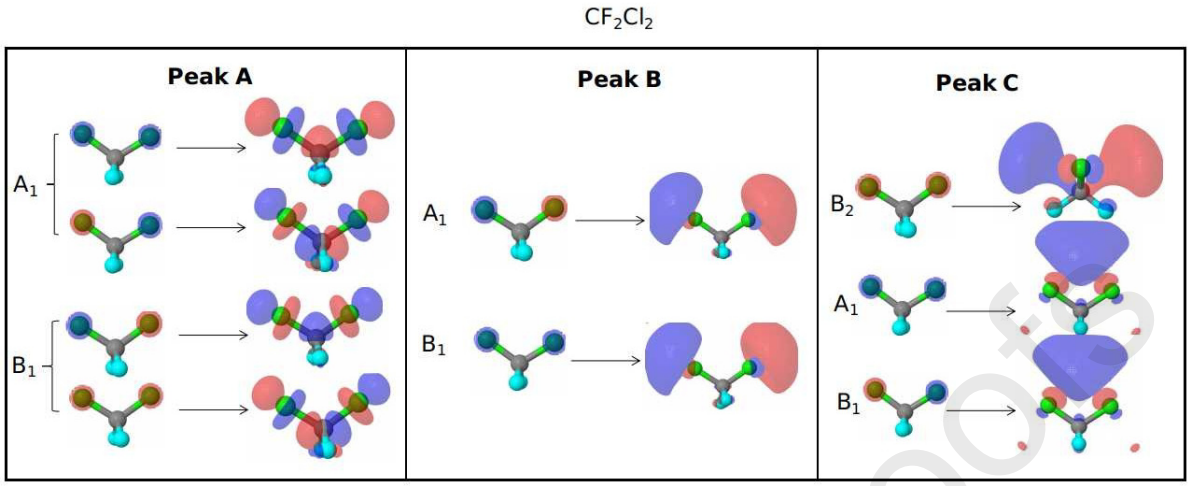

Figure 2: CVS-CCSD NTOs for CF_2Cl_2. Isovalue = 0.04 a.u. for the (particle) valence, 0.03 a.u. for the (particle) Rydberg and 0.001 a.u. for the (hole) core orbitals.

By comparing the fc-CVS-CCSD/aug-cc-pCVDZ K-edge spectrum of CF_2Cl_2 in the presence of the experimental total ion yield (TIY) spectrum by Gomes et al.[32] as presented in Fig. 1, top panel, we observe a good agreement between both results. The intensity of the TIY spectrum, reported in arbitrary units, was scaled to the intensity of the computed oscillator strengths.

The CF_2Cl_2 first strong peak, labeled peak **A**, was computed at 2819.5 eV (See Table 1). We attribute this peak to two degenerate Cl 1s $\rightarrow \sigma^*_{C-Cl}$ states of symmetries A_1 and B_1. The assignments have been done with the help of the CCSD natural transition orbitals[49] which are shown in Figure 2. Natural transition orbitals (NTO) are a simplified way of generating a localized picture of the transition density matrix in terms of hole-particle excitations via separated unitary transformations on the occupied and on the virtual set of orbitals.[49,50] Peak **B**, obtained at 2823.4 eV, is very weak and it is associated with two Rydberg p states of symmetries A_1 and B_1. Peak **C**, obtained at 2824.8 eV, was attributed to a set of Cl 1s $\rightarrow$ Rydberg p states of symmetry B_2, B_1 and A_1. The ionization energies for the states Cl 1s $(1a_1) \rightarrow \infty$ and Cl 1s $(1b_1) \rightarrow \infty$ were both obtained at 2826.8 eV. As one can appreciate from Fig. 2, the final orbitals contributing to peak **A** have a clear C-Cl antibonding character, whereas the final orbitals contributing to peaks **B** and **C** have a Rydberg

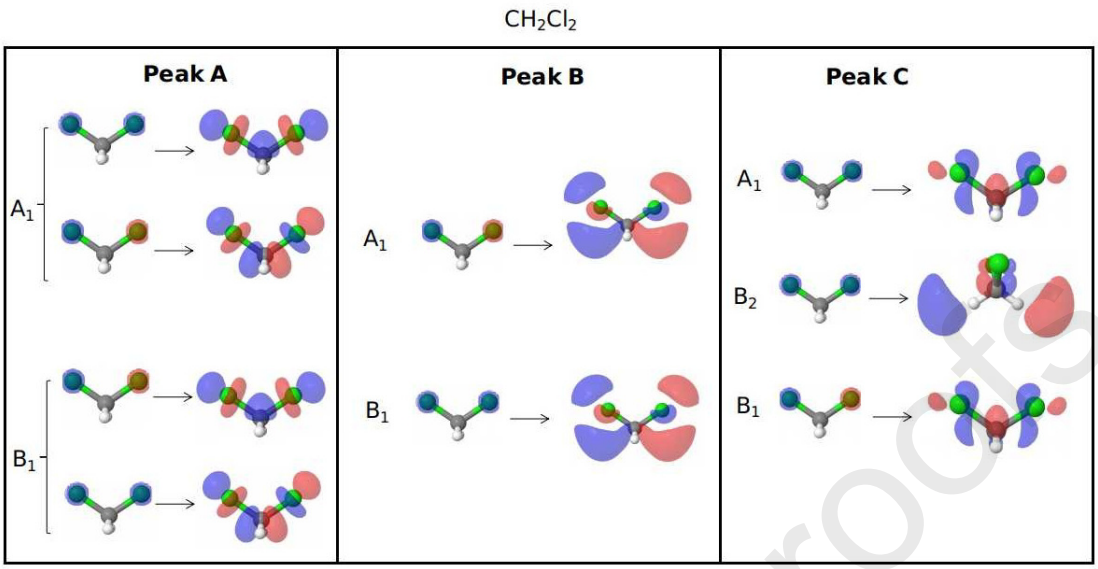

Figure 3: CVS-CCSD NTOs for CH_2Cl_2. Isovalue = 0.04 a.u. for the (particle) valence, 0.03 for the (particle) Rydberg and 0.001 a.u. for the (hole) core orbitals.

p character. Therefore, one can expect a stronger dissociative character for peak **A** than for peaks **B** and **C**.

In order to estimate the influence of the chemical environment on the fragmentation profile of the Cl 1s $\rightarrow \sigma^*$ resonance, we also computed the CH_2Cl_2 spectrum and compared it with the CF_2Cl_2 results.

The states contributing to the NEXAFS spectra of CH_2Cl_2 are presented in Table 2 and plotted alongside with experimental results[11] in Fig. 1, bottom panel. The CH_2Cl_2 NTOs corresponding to the electronic transitions reported in Table 2 are presented in Fig. 3. By comparing the spectra computed for CF_2Cl_2 and CH_2Cl_2, we observe that the first resonance (feature **A** in Fig. 1) is barely influenced by the presence (or absence) of F atoms. The following states contributing to the peaks **B** and **C** in CH_2Cl_2 are redshifted relative to the CF_2Cl_2 spectrum by approximately 1 eV. As in the CF_2Cl_2 case, peak **A** of the CH_2Cl_2 molecule has a strong σ^*_{C-Cl} character and, accordingly, we expect a similar profile for the potential energy surface computed for the first resonance in both the CF_2Cl_2 and the CH_2Cl_2 molecules.

The strong dissociative character of the Cl 1s $\rightarrow \sigma^*_{C-Cl}$ resonance is crucial to the

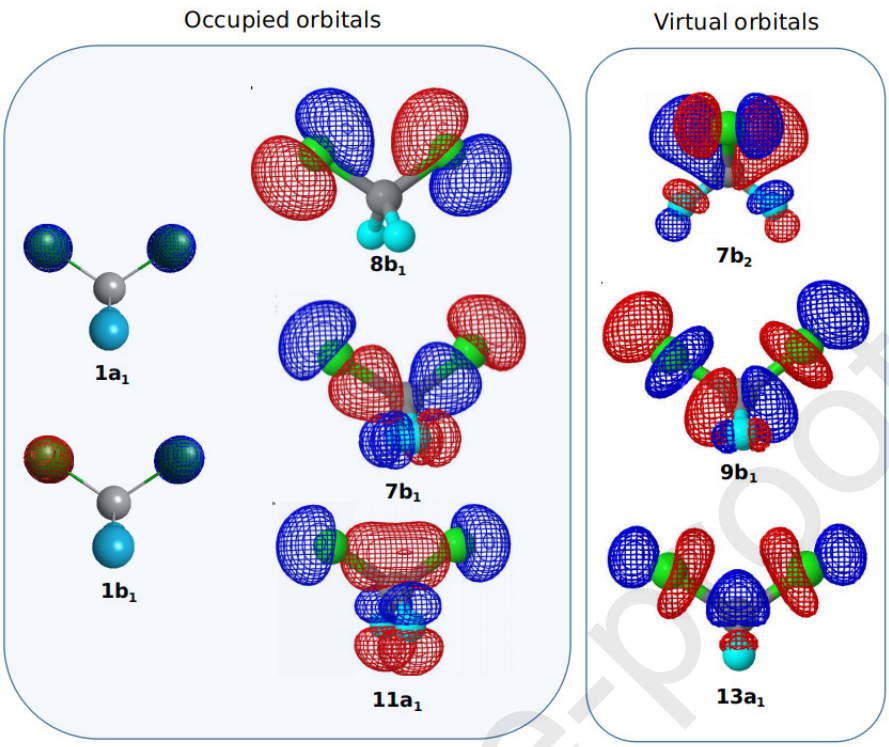

Figure 4: CF_2Cl_2 CASSCF(10,8) active space. Isovalue = 0.05 a.u. for the valence and 0.001 a.u. for the core orbitals.

photofragmentation profile of the CF_2Cl_2 molecule, as measured by Gomes et al.[32] In that study, the authors irradiated the sample with photons of energy ranging from 2819 eV to 2825 eV and measured the partial ion yield (PIY) spectra of each charged fragment and their relative intensity depending on the incident photon energy. For the photon energy equal to 2823 eV (that is, near the Cl 1s $\rightarrow \sigma^*_{C-Cl}$ resonance), the authors observed that the PIY's of the Cl^+ and Cl^{2+} species have inverted behavior. In short, they observed that the dication's yield presents a maximum at 2823 eV, while the cation's yield presents a minimum at the same energy. Based on the σ^*_{C-Cl} character of the first transition, the authors suggested that an increase in the production of neutral chlorine atoms could be related with the dip in the fraction of Cl^+ ions around the first resonance. Also, single and double resonant and normal molecular Auger processes are likely to contribute in the Cl 1s region, but the preference for the dication Cl^{2+} over the cation Cl^+ on the first resonance was not clear. The same trend of a spike in the Cl^{2+} yield coinciding with a fast decrease in the Cl^+ yield at the first Cl 1s

resonance has also been observed experimentally in CH_2Cl_2 (Ref. 11) and CCl_4 (Ref. 31).

Photodissociation at Cl 1s edge

We now analyse the photodissociation profile of the CF_2Cl_2 and CH_2Cl_2 molecules around the Cl K-edge based on the PES's computed at the CASSCF level.

The CASSCF active space for the core-excited and core-ionized potential energy surfaces must be flexible enough to allow for the relaxation of the valence and inner-shell orbitals along the C-Cl bond cleavage due to the core hole excitation/ionization.[14,30,46–48] To ensure this, the CF_2Cl_2 active space was formed by eight orbitals (five occupied and three virtual), chosen as follows: the Cl 1s inner-shell orbitals ($1a_1$ and $1b_1$), three valence orbitals representing the C-Cl bonding ($11a_1$, $7b_1$ and $8b_2$) and three virtual orbitals ($13a_1$, $9b_1$ and $7b_2$). We refer to this active space as IS-CASSCF(10,8). The orbitals selected for the active space of CF_2Cl_2 are shown in Fig. 4. For the calculation of the PES of the ion $CF_2Cl_2^+$, in turn, we used a IS-CASSCF(9,8) space, with 9 electrons in the same eight selected orbitals. For the potential energy surface calculations of CH_2Cl_2 and $CH_2Cl_2^+$, we used an equivalent IS-CASSCF(9,8) active space.

The first Cl 1s excited states of the CF_2Cl_2 molecule computed at the ground state equilibrium geometry with the CASSCF(9,8) active space was obtained at 2818.3 eV. This state (correspondent to the peak **A**) is assigned to the Cl 1s $\rightarrow 13a_1$ and Cl 1s $\rightarrow 9b_1$ orbital transitions. The second core-excited state was obtained at 2821.9 eV and it is assigned mainly to the Cl 1s $\rightarrow 7b_2$ transition. The equivalence among the states computed at the CASSCF and the CCSD levels is evident by comparison of the orbitals labeled $13a_1$ and $9b_1$ of Fig. 4 with the CCSD NTOs for the A_1 and B_1 states contributing to peak A, and of orbital $7b_2$ of Fig. 4 with the CCSD NTO for the Rydberg B_2 state contributing to peak C.

In Fig. 5, top panel, we present the PES for the C-Cl bond cleavage in the CF_2Cl_2 molecule at the Cl 1s $\rightarrow \sigma^*_{C-Cl}$, Cl 1s $\rightarrow$ Rydberg ($7b_2$) and Cl 1s $\rightarrow \infty$ (ion) states. In Fig. 5, bottom panel, we present the forces $\left(-\frac{dE}{dz}\right)$ calculated at the C and Cl positions for

the above mentioned states with respect to the Z-direction, that is, along the C-Cl breaking bond (see inset in Fig. 5).

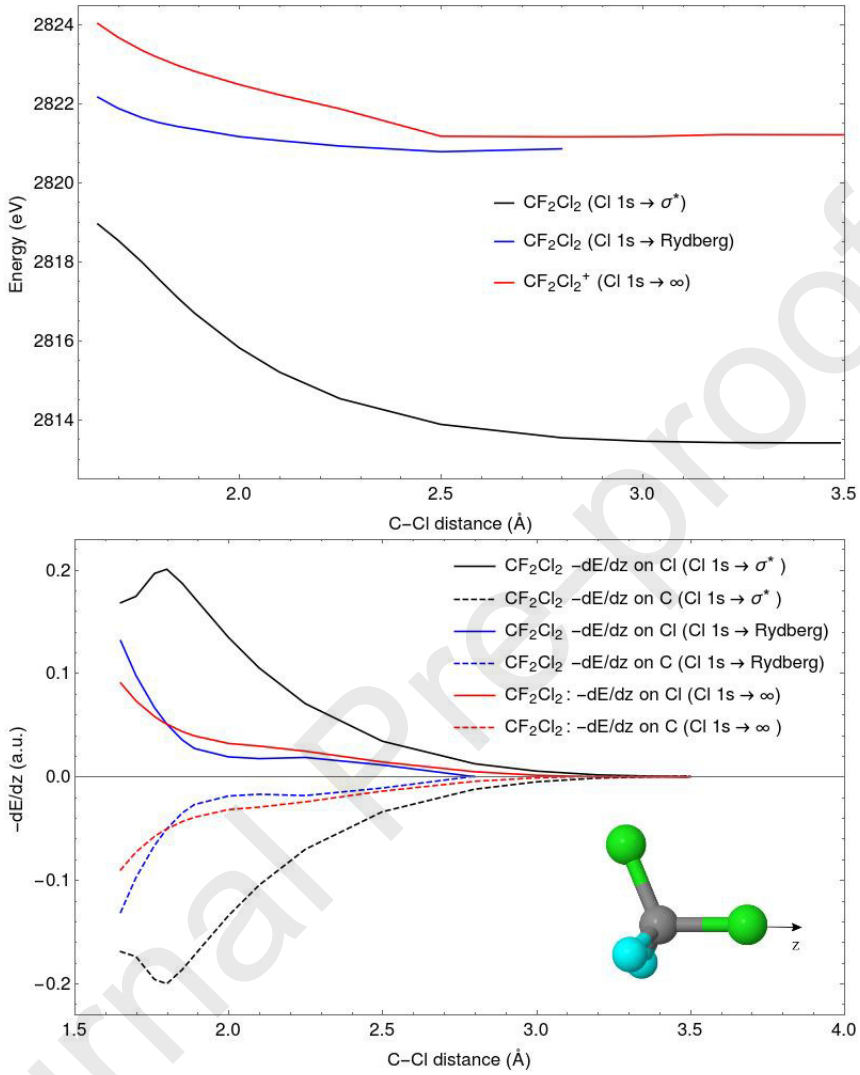

Figure 5: IS-CASSCF(10,8)/aug-cc-pCVDZ potential energy surfaces (top panel) and forces $(-\frac{dE}{dz})$ (bottom panel), calculated on the dissociating Cl and C atoms for the transitions: Cl 1s $\rightarrow \sigma^*_{C-Cl}$, Cl 1s $\rightarrow$ Rydberg and Cl 1s $\rightarrow \infty$ (ion) with respect to the z direction (i.e., along the C-Cl bond cleavage). Notice that the forces on the carbon are opposite to the forces on the leaving chlorine when it comes to a repulsive force on the bond.

The potential energy curves depicted in Fig. 5, show a strong dissociative character for the Cl 1s $\rightarrow \sigma^*_{C-Cl}$ state. The profiles for the Cl 1s $\rightarrow$ Rydberg ($7b_2$) and the Cl 1s $\rightarrow \infty$ (ion) states are, on the other hand, less dissociative. The repulsive behavior of the Cl 1s $\rightarrow \sigma^*_{C-Cl}$ surface is evidenced by the forces $\left(-\frac{dE}{dz}\right)$ acting on the leaving chlorine and the carbon atoms. Near the ground-state equilibrium bond length (1.79 Å), the repulsive force

on the first resonance PES is clearly higher than the ones on Cl 1s → Rydberg ($7b_2$) and the Cl 1s → ∞ PES. The strong repulsive character of the first resonance is also responsible for the maximum observed around 1.79 Å for the state Cl 1s → σ^*_{C-Cl}. In this case, once the C-Cl bond lying along the Z axis contracts, the second Cl atom is expelled relaxing the repulsive force caused by the first chlorine.

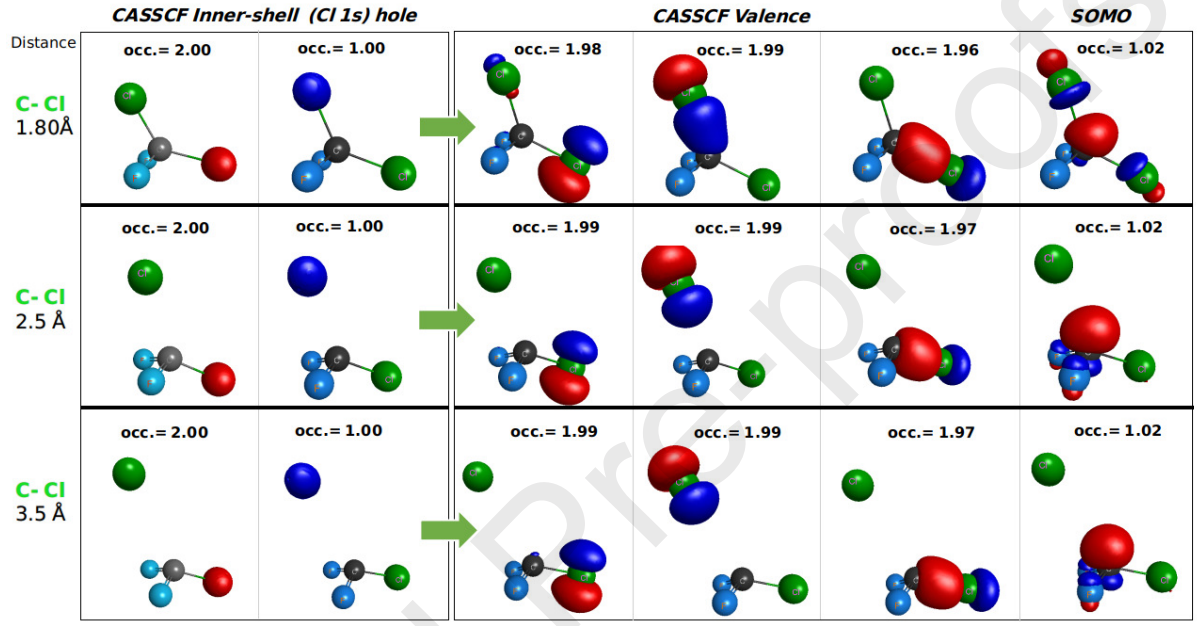

Figure 6: CF_2Cl_2: CASSCF natural orbitals for three representative C-Cl distances along the PES for the resonance Cl 1s → σ^*_{C-Cl}, namely 1.80, 2.50 and 3.50 Å. The natural-orbital occupation numbers are also shown for each orbital. Isovalue = 0.05 a.u. for the valence and 0.001 a.u. for the core orbitals. It is possible to follow the SOMO going from the $13a_1$ molecular orbital (C-Cl distance equal to 1.80 Å) to become a p orbital belonging to the CF_2Cl^* fragment and releasing the Cl^* ($1s^1 2s^2 2p^6 3s^2 3p^6$) atom with the hole on the Cl 1s orbital.

In Fig. 6 we show the occupied natural orbitals[51] and the occupation number for three representative C-Cl distances (1.8, 2.5 and 3.5 Å) along the PES of the CF_2Cl_2 first resonance. For all three C-Cl distances, we observe that the hole is located at the 1s orbital of the leaving Cl atom. The relaxed geometry for the C-Cl distance of 1.8 Å is not symmetric but the single occupied molecular orbital (SOMO) is very similar to the ground state $13a_1$ orbital shown in Fig. 4. The three valence occupied natural orbitals are also similar to the $8b_1$, $7b_1$, and $11a_1$ orbitals of Fig. 4. Going to the C-Cl distance equal to 2.5 Å, it is possible to

observe the breaking of the C-Cl bond, releasing the Cl^* with the hole at the 1s orbital, i.e., with the following electronic configuration $1s^1 2s^2 2p^6 3s^2 3p^6$. Also, one of the valence natural orbitals becomes an occupied Cl 3p atomic orbital and the SOMO becomes a p orbital of the CF_2Cl^* radical with a near trigonal pyramidal geometry. This tendency holds for larger C-Cl distances, such as 3.5 Å, where the C-Cl bond is completely broken. The PES for the Cl 1s $\rightarrow$ Rydberg and ionic states also release the Cl^* ($1s^1 2s^2 2p^6 3s^2 3p^6$) with the hole at the 1s orbital, but the remaining fragments have trigonal planar geometry.

The process illustrated in Fig. 5 and Fig. 6 show the fragmentation of the CF_2Cl_2 molecule generating the $CF_2Cl^{\cdot}$ radical and the $Cl^*(1s^1 2s^2 2p^6 3s^2 3p^6)$ but do not take into account the lifetime of this process. In the ultrafast fragmentation picture, the competitive core-excited relaxation schemes, namely, atomic and molecular Auger decays, take place at the femtosecond time scale.[52,53] Considering the ultrafast dissociation of the C-Cl bond, the $Cl^*(1s^1 2s^2 2p^6 3s^2 3p^6)$ atom can emit Auger electrons after the C-Cl bond cleavage. In this situation, the preference for the multi-charged species is in line with the experimental observations,[11,31,32] where the production of the Cl^{2+} and the Cl^+ species is site-selective.

It is also important to consider the photon energy in a photofragmentation process. Around the Cl K-edge, the amount of energy transferred to the system is high enough to open many decomposition channels generating many charged fragments. Therefore, our results suggest that the channel triggered at the first resonance tends to form unstable $Cl^*(1s^1 2s^2 2p^6 3s^2 3p^6)$ atom by dissociating the C-Cl bond, which rapidly decays to multi-charged chlorine cations via Auger process, which can explain the site selectivity of the fragmentation process.

In Fig. 7, we compared the PES and the forces acting on the leaving Cl and C atoms calculated for the CH_2Cl_2 molecule at the Cl 1s $\rightarrow \sigma^*_{C-Cl}$ and Cl 1s $\rightarrow \infty$ (ion) states with the results of the CF_2Cl_2 equivalent states. It is possible to see that the PES profile of equivalent states is practically the same, showing the influence of fluorine atoms on the PES is small. At the first resonance, the C-Cl cleavage leads to CH_2Cl^* radical also with a near trigonal

pyramidal geometry and the Cl* atom with $1s^1 2s^2 2p^6 3s^2 3p^6$ electronic configuration. This result indicates that the fragmentation mechanism at Cl 1s edge in CH_2Cl_2 is practically the same as the one of CF_2Cl_2.

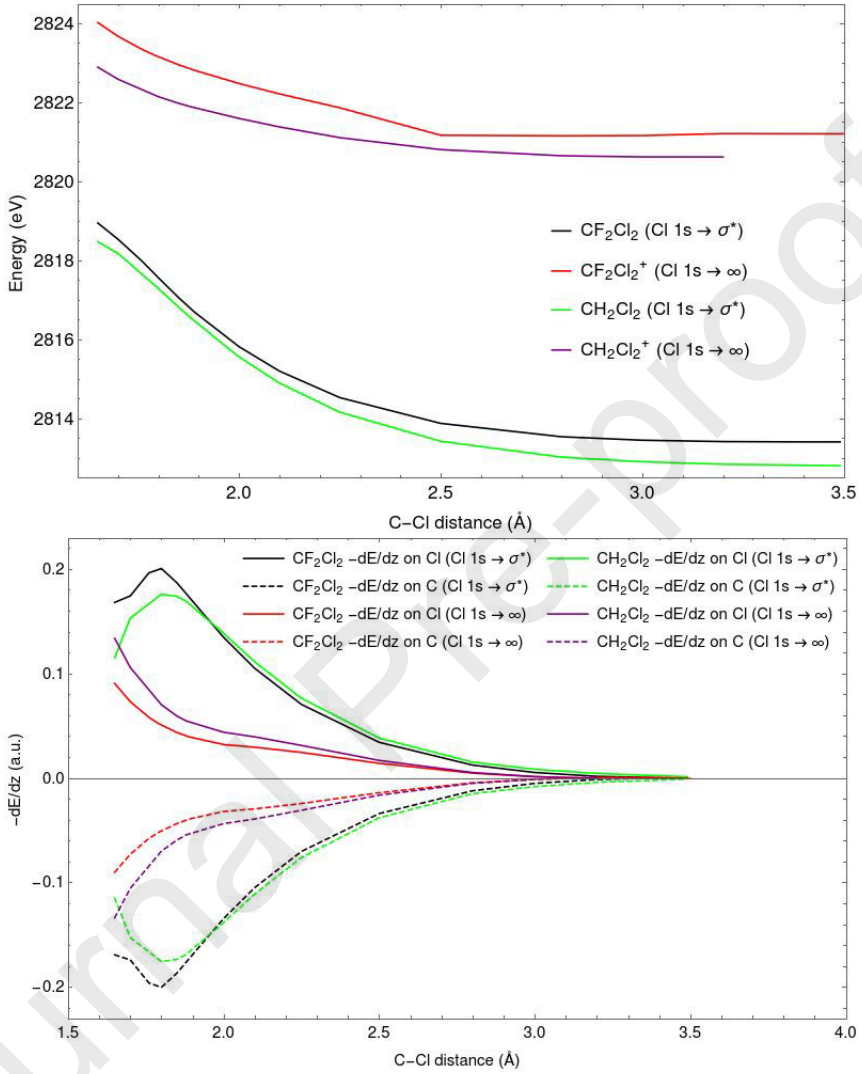

Figure 7: IS-CASSCF(10,8)/aug-cc-pCVDZ PES and forces comparing the CF_2Cl_2 and the CH_2Cl_2 molecules along the C-Cl bond cleavage for the Cl 1s $\rightarrow \sigma^*_{C-Cl}$ resonance and the Cl 1s $\rightarrow \infty$ state (ion).

Conclusions

We presented a theoretical study of the CF_2Cl_2 and CH_2Cl_2 molecules' absorption spectra and photofragmentation profiles at the chlorine K-edge, where site-selective fragmentation

induced by X-rays has been reported.[11,31,32] The first resonance in CF_2Cl_2, corresponding to the Cl 1s $\rightarrow \sigma^*_{C-Cl}$ state, is practically unaffected by the chemical environment, resulting in the same excitation energy and oscillator strength as the Cl 1s $\rightarrow \sigma^*_{C-Cl}$ state in CH_2Cl_2 according to the CCSD calculations. The Rydberg excitations in the CH_2Cl_2 molecule are red shifted by approximately 1 eV with relation to the CF_2Cl_2 molecule.

We have shown that the Cl 1s $\rightarrow \sigma^*_{C-Cl}$ electronic excited state of CF_2Cl_2 tends toward fragmentation into the CF_2Cl^* radical species and the Cl^* ($1s^12s^22p^63s^23p^6$) excited atom, while the Cl 1s $\rightarrow$ Rydberg ($7b_2$) and the Cl 1s $\rightarrow \infty$ states show a weaker tendency to this fragmentation channel. The same holds for CH_2Cl_2, which exhibited the same tendency of fragmentation in the first resonance and ionization state, showing little influence of the chemical environment on both fragmentation profiles.

The amount of energy transferred to the system by irradiation with photons of energy near the Cl K-edge is high enough to open many decomposition channels, hereby generating many charged fragments. Our results suggest that the channel triggered at the first resonance tends to form unstable $Cl^*(1s^12s^22p^63s^23p^6)$ atom by cleavage of the C-Cl bond, which can rapidly decay to multi-charged chlorine cations via atomic Auger process. This fragmentation path can explain the site-selectivity of the multi-charged chlorine fragments.[11,31,32] Moreover, our results indicate that the Cl^+ fragments are mostly produced by fragmentation process after molecular Auger decay channels while multi-charged chlorine cations are produced by atomic Auger relaxation after the C-Cl bond cleavage.

Acknowledgement

R.R.O. acknowledges Conselho Nacional de Desenvolvimento e Pesquisa (CNPq), Coordenação de Aperfeiçoamento de Pessoal de Nível Superior (CAPES), Fundação de Amparo à Pesquisa do Estado do Rio de Janeiro (FAPERJ) for financial support and the National Laboratory for Scientific Computing (LNCC/MCTI, Brazil) for providing HPC resources of the

SDumont supercomputer which has contributed to the research results reported within this paper (http://sdumont.lncc.br). B.N.C.T and S.C. acknowledge financial support from the Independent Research Fund Denmark–Natural Sciences, DFF-RP2 Grant No. 7014-00258B.

References

(1) Inhester, L.; Oostenrijk, B.; Patanen, M.; Kokkonen, E.; Southworth, S. H.; Bostedt, C.; Travnikova, O.; Marchenko, T.; Son, S.-K.; Santra, R.; Simon, M.; Young, L.; Sorensen, S. L. Chemical Understanding of the Limited Site-Specificity in Molecular Inner-Shell Photofragmentation. *The Journal of Physical Chemistry Letters* **2018**, *9*, 1156–1163.

(2) Inhester, L.; Li, Z.; Zhu, X.; Medvedev, N.; Wolf, T. J. A. Spectroscopic Signature of Chemical Bond Dissociation Revealed by Calculated Core-Electron Spectra. *The Journal of Physical Chemistry Letters* **2019**, *10*, 6536–6544.

(3) Schwob, L.; Dörner, S.; Atak, K.; Schubert, K.; Timm, M.; Bülow, C.; Zamudio-Bayer, V.; von Issendorff, B.; Lau, J. T.; Techert, S.; Bari, S. Site-Selective Dissociation upon Sulfur L-Edge X-ray Absorption in a Gas-Phase Protonated Peptide. *The Journal of Physical Chemistry Letters* **2020**, *11*, 1215–1221.

(4) Wernet, P. Chemical interactions and dynamics with femtosecond X-ray spectroscopy and the role of X-ray free-electron lasers. *Philosophical Transactions of the Royal Society A: Mathematical, Physical and Engineering Sciences* **2019**, *377*, 20170464.

(5) Knapp, G. S.; Beno, M. A.; You, H. Hard X-Ray Synchrotron Radiation Applications in Materials Science. *Annual Review of Materials Science* **1996**, *26*, 693–725.

(6) Hirose, M.; Ishiguro, N.; Shimomura, K.; Burdet, N.; Matsui, H.; Tada, M.; Takahashi, Y. Visualization of Heterogeneous Oxygen Storage Behavior in Platinum-Supported Cerium-Zirconium Oxide Three-Way Catalyst Particles by Hard X-ray Spectro-Ptychography. *Angewandte Chemie International Edition* **2018**, *57*, 1474–1479.

(7) Shi, X.; Burdet, N.; Chen, B.; Xiong, G.; Streubel, R.; Harder, R.; Robinson, I. K. X-

ray ptychography on low-dimensional hard-condensed matter materials. *Applied Physics Reviews* **2019**, *6*, 011306.

(8) Attar, A. R.; Bhattacherjee, A.; Leone, S. R. Direct Observation of the Transition-State Region in the Photodissociation of CH_3I by Femtosecond Extreme Ultraviolet Transient Absorption Spectroscopy. *The Journal of Physical Chemistry Letters* **2015**, *6*, 5072–5077.

(9) Attar, A. R.; Bhattacherjee, A.; Pemmaraju, C. D.; Schnorr, K.; Closser, K. D.; Prendergast, D.; Leone, S. R. Femtosecond x-ray spectroscopy of an electrocyclic ring-opening reaction. *Science* **2017**, *356*, 54–59.

(10) Morcelle, V.; Medina, A.; Ribeiro, L. C.; Prazeres, I.; Marinho, R. R. T.; Arruda, M. S.; Mendes, L. A. V.; Santos, M. J.; Tenório, B. N. C.; Rocha, A.; Santos, A. C. F. Fragmentation of Valence and Carbon Core Excited and Ionized CH_2FCF_3 Molecule. *The Journal of Physical Chemistry A* **2018**, *122*, 9755–9760.

(11) Lago, A. F.; Dávalos, J. Z.; Kerdpin, U.; Schlachter, A. S. Cationic and Anionic Fragmentation of Dichloromethane following Inner-Shell (Cl1s) Photoexcitation. *The Journal of Physical Chemistry A* **2006**, *110*, 13717–13723.

(12) Travnikova, O.; Kimberg, V.; Flammini, R.; Liu, X. J.; Patanen, M.; Nicolas, C.; Svensson, S.; Miron, C. On routes to ultrafast dissociation of polyatomic molecules. *Journal of Physical Chemistry Letters* **2013**, *4*, 2361–2366.

(13) Santos, A. C. F.; Vasconcelos, D. N.; MacDonald, M. A.; Sant'Anna, M. M.; Tenório, B. N. C.; Rocha, A. B.; Morcelle, V.; Appathurai, N.; Zuin, L. Atomic versus molecular Auger decay in CH_2Cl_2 and CD_2Cl_2 molecules. *The Journal of Chemical Physics* **2018**, *149*, 054303.

(14) Tenorio, B. N. C.; Kruczkiewicz, F.; de Almeida Ribeiro, F.; Pinho Andrade, D. P.; Riani de Luna, H. M.; Boechat-Roberty, H. M.; Nascimento, M. A. C.; Rocha, A. B.;

Wolff, W. Soft X-ray Chlorine Photolysis on Chlorobenzene Ice: An Experimental and Theoretical Study. *J. Phys. Chem. A* **2019**, *123*, 1389–1398.

(15) Alcantara, K. F.; Rocha, A. B.; Gomes, A. H. A.; Wolff, W.; Sigaud, L.; Santos, A. C. F. Kinetic Energy Release of the Singly and Doubly Charged Methylene Chloride Molecule: The Role of Fast Dissociation. *Journal of Physical Chemistry A* **2016**, *120*, 6728–6737.

(16) Fukuzawa, H. et al. Real-time observation of X-ray-induced intramolecular and interatomic electronic decay in CH_2I_2. *Nature Communications* **2019**, *10*, 2186.

(17) Wolf, T. J. A. et al. Probing ultrafast $\pi\pi^*/n\pi^*$ internal conversion in organic chromophores via K-edge resonant absorption. *Nature Communications* **2017**, *8*, 29.

(18) Tsuru, S.; Vidal, M. L.; Pápai, M.; Krylov, A. I.; Møller, K. B.; Coriani, S. Time-resolved near-edge X-ray absorption fine structure of pyrazine from electronic structure and nuclear wave packet dynamics simulations. *J. Chem. Phys.* **2019**, *151*, 124114.

(19) List, N. H.; Dempwolff, A. L.; Dreuw, A.; Norman, P.; Martínez, T. J. Probing competing relaxation pathways in malonaldehyde with transient X-ray absorption spectroscopy. *Chem. Sci.* **2020**,

(20) Salén, P.; Kamińska, M.; Squibb, R. J.; Richter, R.; Alagia, M.; Stranges, S.; van der Meulen, P.; Eland, J. H. D.; Feifel, R.; Zhaunerchyk, V. Selectivity in fragmentation of N-methylacetamide after resonant K-shell excitation. *Physical Chemistry Chemical Physics* **2014**, *16*, 15231.

(21) Bolognesi, P.; Kettunen, J. A.; Cartoni, A.; Richter, R.; Tosic, S.; Maclot, S.; Rousseau, P.; Delaunay, R.; Avaldi, L. Site- and state-selected photofragmentation of 2Br-pyrimidine. *Physical Chemistry Chemical Physics* **2015**, *17*, 24063–24069.

(22) Cabral Tenorio, B. N.; Kruczkiewicz, F.; De Almeida Ribeiro, F.; Pinho Andrade, D. P.; Riani De Luna, H. M.; Boechat-Roberty, H. M.; Nascimento, M. A. C.; Rocha, A. B.; Wolff, W. Soft X-ray Chlorine Photolysis on Chlorobenzene Ice: An Experimental and Theoretical Study. *Journal of Physical Chemistry A* **2019**, *123*, 1389–1398.

(23) Eberhardt, W.; Sham, T. K.; Carr, R.; Krummacher, S.; Strongin, M.; Weng, S. L.; Wesner, D. Site-specific fragmentation of small molecules following soft-x-ray excitation. *Physical Review Letters* **1983**, *50*, 1038–1041.

(24) Murphy, R.; Eberhardt, W. Site specific fragmentation in molecules: Auger-electron ion coincidence studies on N_2O. *The Journal of Chemical Physics* **1988**, *89*, 4054–4057.

(25) Nenner, I.; Morin, P.; Lablanquie, P.; Simon, M.; Levasseur, N.; Millire, P. Photodissociation of core excited molecules. *Journal of Electron Spectroscopy and Related Phenomena* **1990**, *52*, 623–648.

(26) Lin, Y. S.; Lu, K. T.; Lee, Y. T.; Tseng, C. M.; Ni, C. K.; Liu, C. L. Near-edge X-ray absorption fine structure spectra and site-selective dissociation of phenol. *Journal of Physical Chemistry A* **2014**, *118*, 1601–1609.

(27) Lin, Y. S.; Tsai, C. C.; Lin, H. R.; Hsieh, T. L.; Chen, J. L.; Hu, W. P.; Ni, C. K.; Liu, C. L. Highly Selective Dissociation of a Peptide Bond Following Excitation of Core Electrons. *Journal of Physical Chemistry A* **2015**, *119*, 6195–6202.

(28) Chiang, Y. J.; Huang, W. C.; Ni, C. K.; Liu, C. L.; Tsai, C. C.; Hu, W. P. NEXAFS spectra and specific dissociation of oligo-peptide model molecules. *AIP Advances* **2019**, *9*.

(29) Kokkonen, E.; Jänkälä, K.; Patanen, M.; Cao, W.; Hrast, M.; Bučar, K.; Zitnik, M.; Huttula, M. Role of ultrafast dissociation in the fragmentation of chlorinated methanes. *Journal of Chemical Physics* **2018**, *148*.

(30) Santos, A. C. F.; Vasconcelos, D. N.; MacDonald, M. A.; Sant'Anna, M. M.; Tenório, B. N. C.; Rocha, A. B.; Morcelle, V.; Bonfim, V.; Appathurai, N.; Zuin, L. Evidence of Ultrafast Dissociation in the CHCl3 Molecule. *Journal of Physics B: Atomic, Molecular and Optical Physics* **2020**,

(31) Stolte, W. C.; Santos, A. C.; De Souza, G. G.; Sant'Anna, M. M.; Leung, K. T. Deep-core photoabsorption and photofragmentation of tetrachloromethane near the Cl K-edge. *Journal of Chemical Physics* **2017**, *146*.

(32) Gomes, A.; Wolff, W.; Ferreira, N.; Alcantara, K.; Luna, H.; Sigaud, G.; Santos, A. Deep core ionic photofragmentation of the CF2Cl2 molecule. *International Journal of Mass Spectrometry* **2012**, *319-320*, 1 – 8.

(33) Bohinc, R.; Žitnik, M.; Bučar, K.; Kavčič, M.; Carniato, S.; Journel, L.; Guillemin, R.; Marchenko, T.; Kawerk, E.; Simon, M.; Cao, W. Structural and dynamical properties of chlorinated hydrocarbons studied with resonant inelastic x-ray scattering. *J. Chem. Phys.* **2016**, *144*, 134309.

(34) Björneholm, O.; Sundin, S.; Svensson, S.; Marinho, R. R. T.; Naves de Brito, A.; Gel'mukhanov, F.; Ågren, H. Femtosecond Dissociation of Core-Excited HCl Monitored by Frequency Detuning. *Phys. Rev. Lett.* **1997**, *79*, 3150–3153.

(35) Céolin, D.; Piancastelli, M. N.; Stolte, W. C.; Lindle, D. W. Partial ion yield spectroscopy around the Cl 2p and C 1s ionization thresholds in CF_3Cl. *The Journal of Chemical Physics* **2009**, *131*, 244301.

(36) Liu, X. J.; Prümper, G.; Kukk, E.; Sankari, R.; Hoshino, M.; Makochekanwa, C.; Kitajima, M.; Tanaka, H.; Yoshida, H.; Tamenori, Y.; Ueda, K. Site-selective ion production of the core-excited CH_3F molecule probed by Auger-electron–ion coincidence measurements. *Physical Review A* **2005**, *72*, 042704.

(37) Lu, K. T.; Chen, J. M.; Lee, J. M.; Haw, S. C.; Chen, S. A.; Liang, Y. C.; Chen, S. W. State-selective enhanced production of positive ions and excited neutral fragments of gaseous CH_2Cl_2 following Cl $2p$ core-level photoexcitation. *Phys. Rev. A* **2010**, *82*, 033421.

(38) Coriani, S.; Koch, H. Communication: X-ray absorption spectra and core-ionization potentials within a core-valence separated coupled cluster framework. *J. Chem. Phys.* **2015**, *143*, 181103.

(39) Coriani, S.; Koch, H. Erratum: "Communication: X-ray absorption spectra and core-ionization potentials within a core-valence separated coupled cluster framework" [J. Chem. Phys. 143, 181103 (2015)]. *J. Chem. Phys.* **2016**, *145*, 149901.

(40) Vidal, M. L.; Feng, X.; Epifanovsky, E.; Krylov, A.; Coriani, S. A New and Efficient Equation-of-Motion Coupled-Cluster Framework for Core-Excited and Core-Ionized States. *J. Chem. Theory Comput.* **2019**, *15*, 3117–3133.

(41) Werner, H.; Knowles, P. J. A second order multiconfiguration SCF procedure with optimum convergence. *The Journal of Chemical Physics* **1985**, *82*, 5053–5063.

(42) Linstrom, P.; Mallard, W. NIST Chemistry WebBook, NIST Standard Reference Database. 2017; `http://webbook.nist.gov`.

(43) Werner, H.-J.; Knowles, P. J.; Knizia, G.; Manby, F. R.; Schütz, M. Molpro: a general-purpose quantum chemistry program package. *WIREs Comput Mol Sci* **2012**, *2*, 242–253.

(44) Shao, Y. et al. Advances in molecular quantum chemistry contained in the Q-Chem 4 program package. *Molecular Physics* **2015**, *113*, 184–215.

(45) Dunning, T. H.; Peterson, K. A.; Wilson, A. K. Gaussian basis sets for use in correlated

molecular calculations. X. The atoms aluminum through argon revisited. *J. Chem. Phys.* **2001**, *114*, 9244.

(46) Rocha, A. B. Potential curves for inner-shell states of CO calculated at multiconfigurational self-consistent field level. *J. Chem. Phys.* **2011**, *134*, 024107.

(47) Tenorio, B. N. C.; de Moura, C. E.; Oliveira, R. R.; Rocha, A. B. Transitions energies, optical oscillator strengths and partial potential energy surfaces of inner-shell states of water clusters. *Chem. Phys.* **2018**, *508*, 26 – 33.

(48) Santos, A. C. F.; Vasconcelos, D. N.; MacDonald, M. A.; Sant'Anna, M. M.; Tenorio, B. N. C.; Rocha, A. B.; Morcelle, V.; Appathurai, N.; Zuin, L. Atomic versus molecular Auger decay in CH2Cl2 and CD2Cl2 molecules. *The Journal of Chemical Physics* **2018**, *149*, 054303.

(49) Martin, R. L. Natural transition orbitals. *The Journal of Chemical Physics* **2003**, *118*, 4775–4777.

(50) Krylov, A. I. From orbitals to observables and back. *The Journal of Chemical Physics* **2020**, *153*, 080901.

(51) Davidson, E. R. In *Natural Orbitals*; Löwdin, P.-O., Ed.; Advances in Quantum Chemistry; Academic Press, 1972; Vol. 6; pp 235 – 266.

(52) Kivimaki, A.; Alvarez-Ruiz, J.; Wasowicz, T. J.; Callegari, C.; de Simone, M.; Alagia, M.; Richter, R.; Coreno, M. O 1s excitation and ionization processes in the CO2 molecule studied via detection of low-energy fluorescence emission. *Journal of Physics B: Atomic, Molecular and Optical Physics* **2011**, *44*, 165103.

(53) Kokkonen, E.; Jänkälä, K.; Patanen, M.; Cao, W.; Hrast, M.; Bučar, K.; Žitnik, M.; Huttula, M. Role of ultrafast dissociation in the fragmentation of chlorinated methanes. *J. Chem. Phys.* **2018**, *148*, 174301.